Valence-band electronic structure of MoS_2 and $Cs/MoS_2(0002)$ studied by angle-resolved x-ray photoemission spectroscopy

Ken T. Park, Michelle Richards-Babb,* James S. Hess, Jeff Weiss, and Kamil Klier
Zettlemoyer Center for Surface Studies and Department of Chemistry, Lehigh University, Bethlehem, Pennsylvania 18015
(Received 26 February 1996)

The angle dependence of the valence-band photoemission from the trigonal prismatic layered MoS_2 shows both the forward-scattering features normally observed in core-level photoelectron diffraction and, in addition, the *initial-state orbital character associated with partially occupied, nonbonding* $Mo^{IV}(4d_{z^2}+4d_{x^2-y^2}+4d_{xy})$ *orbitals near the top of the valence band.* The difference in forward scattering between the Mo and S emitters is also used to assess relative contributions from the Mo and S atomic orbitals at specific binding energies within the valence band. Deposition of cesium (0.23 ML Cs with 1 ML equal to the Cs saturation coverage) onto the basal plane of MoS_2 introduces a density of states at 1.25 eV above the top of the valence-band maximum. The intensity anisotropy for this Cs-induced valence level is interpreted via the angle dependence of the electric dipole matrix element as due to the initial-state orbital character at the bottom of the conduction band of the Cs/MoS_2 heterostructure. [S0163-1829(96)06632-5]

I. INTRODUCTION

Since the early observation of angular anisotropy of valence-band (VB) photoelectrons reported by Siegbahn *et al.* in 1970,[1] electron spectroscopy was recognized to encompass information on both electronic and structural properties of solids and their surfaces. The photoemission process has been analyzed in terms of models, some of which divide this process into a sequence of individual events. The most widely adopted ''three-step'' model considers photoionization, propagation of photoelectrons in solids, and the transmission through the vacuum-solid interface as separate and independent processes. In this model, the photoelectron intensity is expressed as[2]

$$I(E,\mathbf{k}) \propto \sum_{fi} \int_{\mathrm{BZ}} d^3\hat{k}_i |M_{\mathrm{fi}}|^2 \delta(\mathbf{k}-\mathbf{k}_i-\mathbf{G}-\mathbf{k}_{\mathrm{ph}}) \times \delta(E-E_i-\hbar\omega) DT. \quad (1)$$

The electric dipole matrix element M_{fi} can be written as $\langle f|\hat{\varepsilon}\cdot\hat{r}|i\rangle$ between the initial state $|i\rangle$ of energy E_i and momentum $\hbar\mathbf{k}_i$, and the final state $|f\rangle$ of energy E and momentum $\hbar\mathbf{k}$, where $\hat{\varepsilon}$ is the photon polarization vector and $\hat{r}$ is the position operator. $\mathbf{k}_{\mathrm{ph}}$ is the wave vector of an impinging x-ray photon. The first δ function in Eq. (1) is the momentum conservation term, the second δ function the energy conservation term, $\mathbf{G}$ is a reciprocal-lattice vector, and D and T are the second and third steps of the three-step photoemission. When the VB is probed by x-ray photoelectron spectroscopy (XPS), the kinetic energy of the photoelectrons is large ($\approx$1480 eV using Al $K\alpha$ radiation) such that even high angular resolution of state-of-the-art analyzers, $\Delta\theta \leqslant 4°$ gives rise to relatively large uncertainty in momentum $\Delta\mathbf{k}$.[3] In this case, the entire Brillouin zone (BZ) is sampled, and Eq. (1) upon integration over all values of $\mathbf{k}_i$ reduces to

$$I(E,\mathbf{k}) \propto N(E_i)N(E)|M_{\mathrm{fi}}|^2 DT, \quad (2)$$

where $N(E_i)$ and $N(E)$ are the densities of the initial and final states, respectively. Depending upon the model and the definition of the wave functions, it is always possible to include parts of the initial- or final-state wave functions into the matrix element or the density of states. In the *matrix element model*,[4,5] the angular dependence originates from the combination of the initial and final states in M_{fi}. Assuming that the final state is a plane wave, it was shown that the squared matrix element $|M_{\mathrm{fi}}|^2$ can be reduced to the probability density of the initial state orbital $|\Sigma_m c_m Y_{lm}(\theta_k,\varphi_k)|^2$, where c_m are the coefficients that form real orbitals, and θ_k and φ_k are the spherical polar coordinates of the photoelectron momentum vector.[6] However, the plane-wave approximation was later turned aside because of concerns about its validity. Gadzuk[7] and Goldberg, Fadley, and Kono[8] derived theoretical expressions for angle dependence of M_{fi} using a more accurate form of the final states. In the *direct transition model*, on the other hand, only those states connected by the wave vector and energy conservation contribute to the intensity. To explore the angular variation due to the wave vector and energy conservation, one version of the direct transition model assumed that the matrix elements M_{fi} are independent of the emission angle.[9,10] Thus the anisotropy in this model arises from the fact that different parts of the BZ are sampled along different directions, but not from angular variations of the transition matrix element.

In addition to the intensity anisotropy due to the photoexcitation process, an anisotropy of the VB photoelectron intensity may also arise from electron transport through the crystal lattice via term D in Eq. (1). It was not until a few years ago that intensity anisotropy of the VB photoelectrons due to scattering process was observed using angular resolution of $\Delta\theta \leqslant 3°$, where the highly delocalized VB photoelectrons in Al(001) exhibited a forward-scattering x-ray photoelectron diffraction (XPD) pattern very similar to that of a well-localized level.[11] This study naturally raised a question where the similarity between the core level and VB XPD's ends. Although Herman *et al.*[12] recently showed that fine

differences in XPD between the VB and core levels could occur depending on the degree to which the direct transition effect contributed, no such differences between the core level and VB XPD due to the contribution from the matrix element have been reported, to our knowledge.

In this work, we examine relative contributions to VB photoelectron intensity anisotropy due to the diffraction and shape of the initial-state valence orbitals in the layered trigonal prismatic 2-*H* molybdenum disulfide. Subsequently we investigate the VB electronic structure after Cs adsorption on the $MoS_2(0002)$ surface. This study is motivated by the following: (i) the MoS_2 VB structure is relatively well understood,[13,14] stemming from the filled S $3s$ and S $3p$ and partially filled Mo $4d$ orbitals; (ii) the dispersion in MoS_2 is large ($\simeq 1$ eV at the top of the VB and up to 1.3 eV in the middle and the bottom of the VB),[13,14] which affords a test of whether VB XPS samples the entire BZ, in which case VB peak positions will be independent of the emission angle θ, or portions of BZ such that the peak positions will change with θ over the dispersion range; (iii) the MoS_2 crystals are stoichiometric and structurally robust as well as anisotropic, and do not undergo surface reconstruction or relaxation; (iv) the use of photoemission from two elements (Mo and S) as well as their VB and core levels permits comparisons between emitters at different locations and between spherically symmetric, filled shells and nonspherically symmetric, partially filled shells; and (v) the cesium adsorption on clean MoS_2 is of fundamental interest in surface science as well as of technological importance in catalysis.[14]

II. EXPERIMENTAL PART

All $MoS_2(0002)$ single crystals investigated in this study were in the form of the natural mineral molybdenite, obtained from Ward's Natural Science Establishment. For all samples studied in this experiment, a clean, well-ordered surface of $MoS_2(0002)$ was obtained by peeling off the top surface layers inside a glove bag, filled with N_2. The glove bag was attached to the fast entry chamber of the SCIENTA ESCA (electron spectroscopy for chemical analysis) ultrahigh-vacuum (UHV) chamber, so that the freshly peeled samples were immediately transferred to the UHV system without exposing them to atmosphere. The surface order of $MoS_2(0002)$ was verified with low-energy electron diffraction by observing sharp $p(1\times1)$ LEED spots. The survey XPS spectrum showed carbon as a minor surface impurity, and from the XPS measurements the ratio of sulfur to carbon atoms was found to be approximately 3.0, higher than what one would expect from the near-perfect low-energy electron-diffraction (LEED) pattern. However, further analysis by atomic resolution scanning tunneling microscopy images revealed that carbon impurity was in clustered form, leaving most of the basal plane atomically flat.[15] In the second set of experiments, cesium was evaporated onto the basal plane of the MoS_2 at room temperature using a commercially available SAES getter source. The total Cs exposure time was gradually incremented by 3 min, until no further increase in the Cs $3d_{5/2}$ core-level intensity was observed after 24 min of the total Cs exposure time. During the study, the base pressure of the analysis chamber remained in low 10^{-10} mbar, and no significant increase in the contamination level was observed.

The XPD data were obtained using the SCIENTA ESCA-300 spectrometer, which employs a rotating anode to generate a high power monochromatized and unpolarized Al $K\alpha$ line. The excited photoelectrons were detected by a 300-mm mean radius hemispherical electron energy analyzer fixed at 45 ° from the x-ray source.[15,16] The combination of the high power, monochromatized x-ray radiation and the hemispherical energy analyzer provides experimental energy resolution ~ 0.24 eV, judging from the width of the Au Fermi level. The sample was mounted on a manipulator which allows three degrees of translational and two degrees of rotational motion of the sample. The polar angle XPS scans were obtained at 1 ° intervals from -10 ° to 70 ° measured from the surface normal along $\langle 11\bar{2}0\rangle$ (hereafter $\phi = 90$ °) with an angular resolution of ≈ 4 ° mainly estimated by the acceptance angle of the detector. Both the VB and the Mo $3d_{5/2}$ spectra were recorded at each polar angle θ in order that the XPD of the Mo $3d_{5/2}$ core level could be used as reference for the VB XPD. Detailed information about the spectrometer and angle resolved x-ray photoemission spectroscopy (ARXPS) geometry can be found elsewhere.[15,16]

III. RESULTS

The polar angle scan of raw VB spectra of the $MoS_2(0002)$ crystal along $\phi = 90$ ° is presented in Fig. 1(a). Each VB spectrum showed inner VB S $3s$ and five distinct outer VB components which are labeled as A–E. The peak positions were *strictly* independent of the polar angle θ, and their binding energies (BE's) were A, 2.5 eV; B, 3.8 eV; C, 5.1 eV; D; 5.9 eV; and E, 7.1 eV. In sharp contrast with the present results, the recent angle-resolved ultraviolet photoemission spectroscopy (ARUPS) experiment with the $MoS_2(0002)$ surface along the same crystallographic direction and over similar range of polar angles[13] showed that the dispersion is large (≈ 1 eV) in MoS_2, as demonstrated by the strong angle dependence of all bands. The general XPD patterns of the outer VB peaks were similar to those of the Mo $3d$ core and S $3s$ levels, regardless of the VB peak positions, and all VB XPD's exhibited strong forward focusing maxima at $\theta = 0$ ° and 49 ° corresponding to the internuclear axes of the nearest and next-nearest neighbors.[15,17]

The intensity variations of the outre VB peaks are further compared with those of the Mo $3d_{5/2}$ core and S $3s$ levels in order to examine the VB XPD features in greater detail [Fig. 1(b)]. The intensities of all VB's as well as the core-level peaks were obtained by integrating the area under the peaks after the background was subtracted.[18] Although all VB XPD's exhibited forward focusing maxima similar to the core levels, they revealed the following fine differences among the VB components: first, peak A showed strong attenuation at higher exit angles θ, while all other VB peaks displayed relatively flat background; in addition, the forward focusing maxima at $\theta = 49$ ° for peaks B and C were larger than those at 0 ° in the XPD pattern observed in the Mo $3d_{5/2}$ core level, while VB peak E and S $3s$ showed less intense maxima at $\theta = 49$ °.

The first 3 min of Cs evaporation on a clean $MoS_2(0002)$ surface produced the Cs $5p_{3/2}$ level at BE

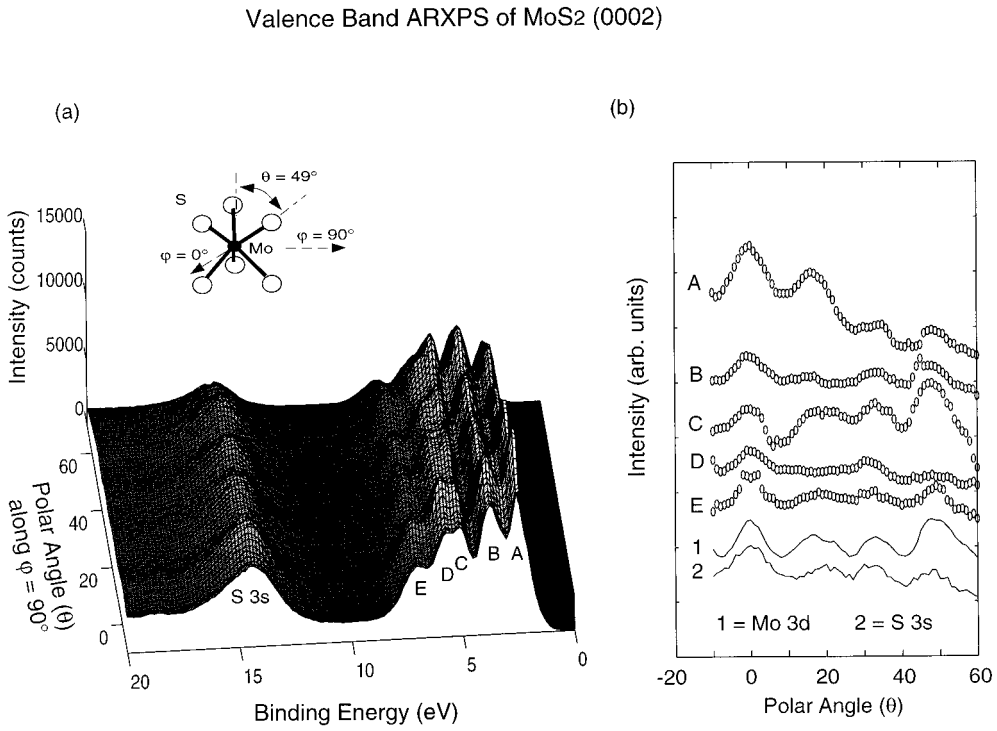

FIG. 1. (a) Polar angle scan of 81 VB spectra from $MoS_2(0002)$ along $\phi = 90°$ ($\langle 11\bar{2}0 \rangle$ azimuth) from $\theta = -10° - 70°$ at room temperature. Also shown is the trigonal prismatic structure of MoS_2 (top). (b) Detailed XPD patterns of each outer VB peaks A–E are compared to those of the Mo $3d_{5/2}$ core and the S $3s$ level (line plots 1 and 2, respectively).

$=11.94$ eV, partly overlapped with the S $3s$ level of the substrate [Fig. 2(a)]. In addition, another Cs-induced density of states appeared at 2.15 eV above the VB peak A (or approximately 1.25 eV above the top of the valence band). The position of this peak was near that of the Cs $6s$ valence level reported for Cs metal using UPS,[19] thus we initially assigned this peak as the Cs $6s$ valence level. The steady increase in the Cs exposure time resulted in an increase in photoemission intensity from various Cs electronic levels including the Cs $5p$ and Cs $3d$ levels up to 24 min of the total Cs exposure time [Fig. 2(b)]. When Cs was evaporated for a total of 24 min, both the Cs $5p_{3/2}$ and Cs $5p_{1/2}$ peaks were well resolved with a spin-orbit splitting of $\Delta E = 1.60$ eV, and the Cs $5p_{3/2}$ peak was shifted by about 0.2 eV toward the Fermi level. Similarly, the peak position for the Cs $3d_{5/2}$ core level was measured at 726.02 eV after 3 min of Cs exposure, and shifted toward the Fermi level by ~ 0.3 eV as the Cs exposure time increased. The peak positions of the Cs $3d_{5/2}$ core level were found well within the range of the reported peak positions of the Cs $3d_{5/2}$ core level from cesium metal.[20] From a comparison between the intensity of the Cs $3d_{5/2}$ peak after 3 and 24 min of exposure, the coverage of the

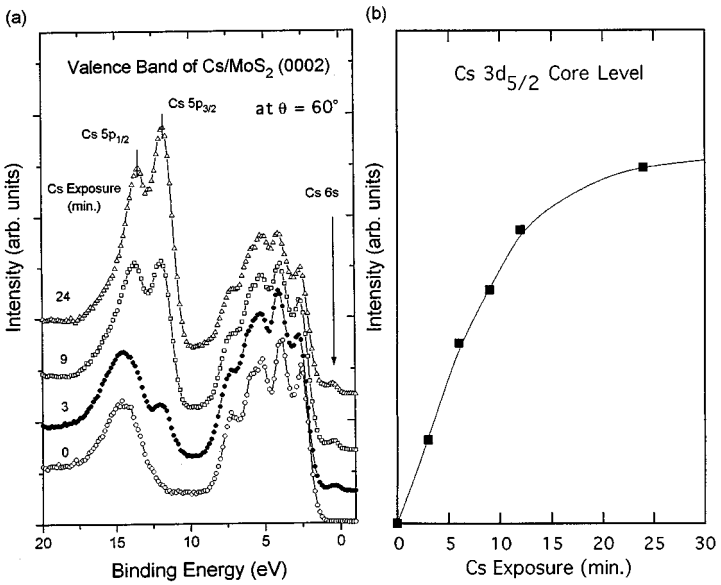

FIG. 2. (a) The changes in the VB spectrum taken at $\theta = 60°$ during the formation of the Cs overlayer on the $MoS_2(0002)$ surface after various Cs exposure times: 0 (clean), 3, 9, and 24 min. (b) The intensity of the Cs $3d_{5/2}$ core level was plotted against the Cs exposure time.

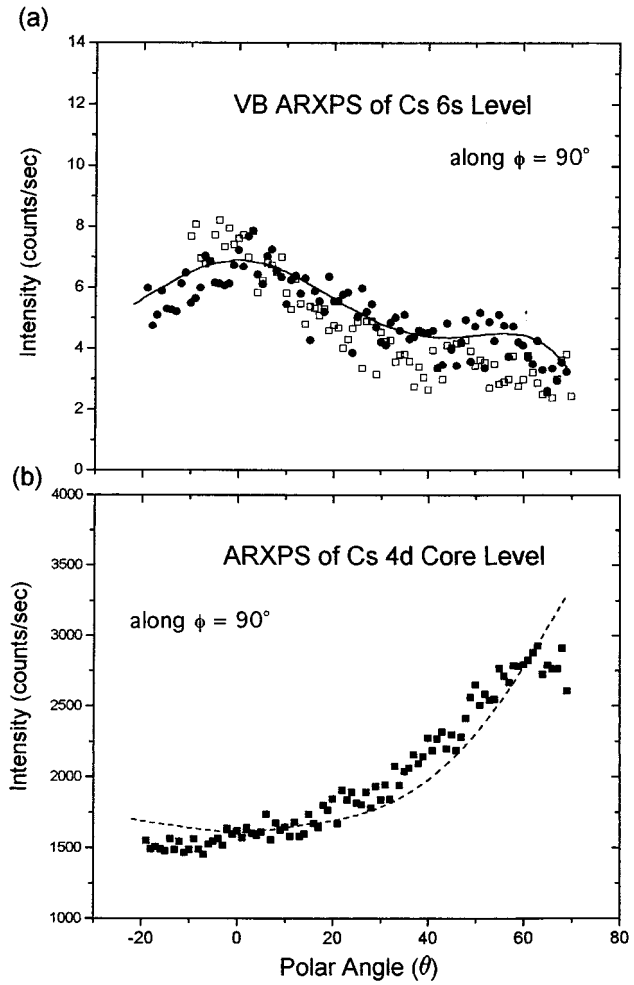

FIG. 3. (a) VB ARXPS of the Cs 6*s* level at 0.23-ML Cs coverage (equivalent to 3-min Cs exposure, open squares). A separate experiment with 0.22-ML Cs coverage on $MoS_2(0002)$ using a wider range of polar angles ($\theta = -22° - 70°$) reproduced the intensity anisotropy of the Cs 6*s* level (full circles). (b) ARXPS of the Cs 4*d* core level at 0.22-ML Cs coverage (full squares). The solid line in (a) and the dashed line in (b) represent theoretical accounts for the observed ARXPS data (see Sec. IV).

adsorbed Cs after 3-min Cs evaporation was determined to be 0.23 ML, where 1 ML is defined to be the Cs saturation coverage.

The θ dependence of the x-ray photoelectron intensity from the Cs 6*s* level is presented in Fig. 3(a) (open squares). The intensities at each angle were obtained as peak areas after subtracting background intensities before Cs evaporation [the bottom curve in Fig. 2(a)]. The θ dependence of the Cs 6*s* level showed a striking intensity anisotropy: a broad intensity maximum along the surface normal, slowly decreasing toward higher polar angles. A similar experiment after 0.22-ML Cs deposition on the $MoS_2(0002)$ using a wider polar angle range from $\theta = -22° - 70°$ successfully reproduced the observed polar angle dependence of the Cs 6*s* photoemission more clearly, depicting a broad maximum at $\theta = 0°$ [filled circles in Fig. 3(a)]. In contrast to the Cs 6*s* level, the angle dependence of the Cs 4*d* core electron intensity exhibited a smoothly increasing intensity profile [Fig. 3(b)].

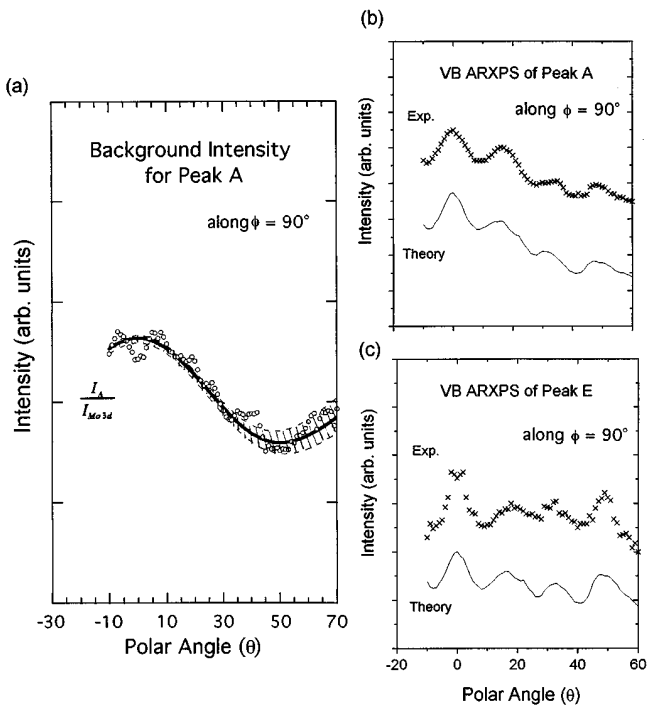

FIG. 4. (a) The VB ARXPS data for *A* is divided by the experimental XPD of the Mo $3d_{5/2}$ core level to show the distinctive behavior in the background intensity of peak *A*. The background intensity anisotropy is compared with the calculated angle dependence of the matrix elements. Comparison between the experimental VB ARXPS and the simulated VB XPS after multiplying the intensity anisotropy due to the matrix elements by the Mo $3d_{5/2}$ core-level XPD patterns for (b) peak *A* and (c) peak *E*.

IV. DISCUSSION

A. Valence-band structure, photoelectron diffraction, and effects of matrix elements in ARXPS of bare MoS_2

The intensity variation at the top of the valence band (peak *A*) with the angle θ is in sharp contrast to that of other peaks, displaying a substantial decrease in background intensity near $\theta = 50°$ [Fig. 1(b)]. To examine the angle dependence of the background intensity for peak. A more carefully, the instrument response function and intensity modulation due to forward focusing were removed by dividing the VB ARXPS data of peak *A* by the XPD of the Mo $3d_{5/2}$ core level [Fig. 4(a)]. The resulting background intensity profile for peak *A* clearly exhibits a maximum at $\theta = 0°$ and a minimum near $\theta = 50°$, roughly similar to the shape of the initial-state atomic orbital $d_{z^2} \propto (3\cos^2\theta - 1)$. A similar intensity minimum near $\theta = 50°$ for peak *A* was previously reported by Williams, Kemeny, and Ley,[5] who qualitatively assigned the intensity anisotropy to the initial-state characteristic of the Mo d_{z^2} orbital. However, the study did not report the core-electron-like XPD as well as the maximum at 0°, perhaps due to are relatively large angular step ($\Delta\theta > 3°$) incorporated in the polar angle scan from $\theta = 20°$ to 78°. In contrast, the accuracy in the polar angle scan in the present study was better than 1°, judging from the positions of the forward focusing maxima of the core levels. Therefore, the fact that the observed minimum for peak *A* neither reached zero nor occurred exactly at

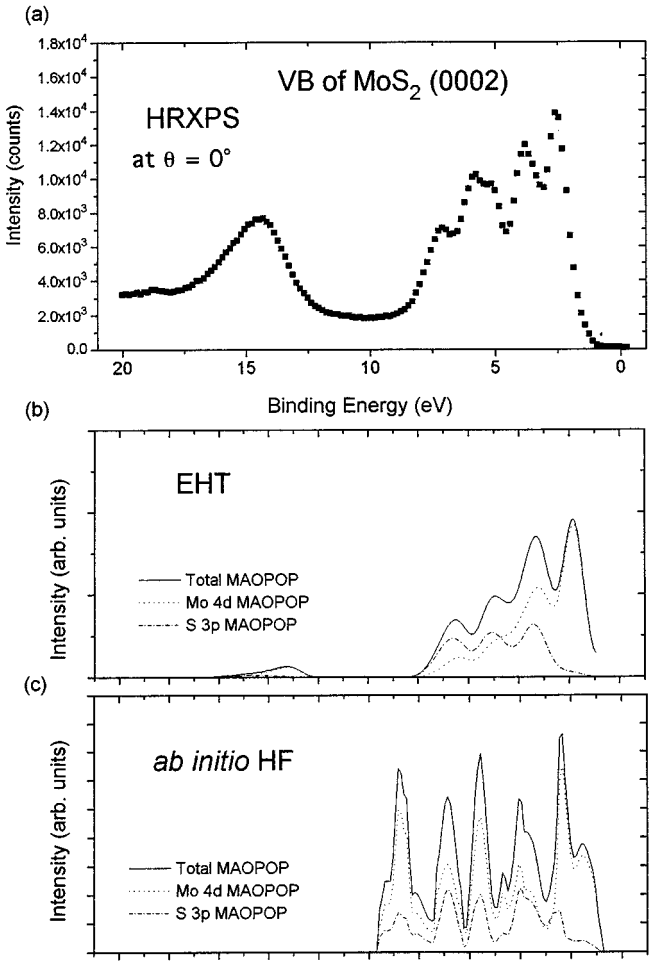

FIG. 5. The comparison in the density of states among (a) the experimental VB XPS at $\theta=0°$, (b) the solid-state extended Hückel theory, and the (c) *ab initio* Hartree-Fock calculation using the linear combination of atomic orbitals.

$\theta=54°$, the nodal angle of the d_{z^2} orbital, suggested additional contributions from orbitals other than d_{z^2}. Indeed, using the solid-state extended Hückel theory (SSEHT), a recent theoretical analysis of the VB structure of MoS_2 in terms of the modified atomic orbital population (MAOPOP) (Ref. 21) showed that peak A was mainly composed of Mo $4d$ atomic orbitals (Fig. 5) and further predicted the ratio of $d_{z^2}:d_{xy}:d_{x^2-y^2}=0.52:\ 0.26:\ 0.22$ for the relative atomic-orbital population.[22] More recently, *ab initio* Hartree-Fock calculation using Hay-Wadt's effective core pseudopotential for a Mo atom and the all-electron basis set for a S atom also confirmed such a dominance of the Mo d_{z^2} orbital character at peak A, successfully reproducing the band structure calculated by the earlier SSEHT.[23] An accurate measurement of the background intensity variation in this study and the calculation of the VB structure of MoS_2 enabled us to make a quantitative assessment of the contributions from various atomic orbitals, and compare the result with theory.

If the initial Bloch wave function is expressed as a linear combination of atomic orbitals, the electric dipole matrix element in Eq. (1) can be rewritten as a triple product of spherical harmonics using the initial atomic orbital $\phi_{nl}(r,\theta,\varphi)=R_{nl}(r)\Sigma_m c_m Y_{lm}(\theta,\varphi)$ and the final-state wavefunction[7,8]

$$\phi_{E,\mathbf{k}}(r,\theta,\varphi) = 4\pi\sum_{l'm'} i^{l'}e^{-i\delta_l}Y^*_{l'm'}(\theta_k,\varphi_k)Y_{lm}(\theta,\varphi)R_{E,l'}(r)$$

where $R(r)$ and $Y(\theta,\varphi)$ are the radial part and spherical harmonics for the wave functions and δ_l is the phase shift for the lth partial wave due to the hole potential. Goldberg, Fadley, and Kono[8] have shown that the squared matrix element $|M_{\mathrm{fi}}|^2$ can be reduced to a calculation-ready expression containing geometric parameters of the experiment. This method was used in the present analysis of intensity variation of peak A initial-state orbitals $d_{z^2}(l=2,m_l=0)$, and d_{xy}, $d_{x^2-y^2}(l=2,m_l=\pm2)$ to the final states of the p and f channels subject to the dipole selection rules $\Delta l=\pm1$ and $\delta m_l=\pm1,\ 0$. The experimental anisotropy of peak A was fitted with a linear combination of the squared matrix elements for each initial orbital to yield the ratio of d_{z^2}: d_{xy}: $d_{x^2-y^2}=0.51:\ 0.24:\ 0.25$ [a solid line in Fig. 4(a)], in excellent agreement with the theoretical values. As the ratio of d_{z^2}: d_{xy}: $d_{x^2-y^2}$ changes from 0.56: 0.21: 0.22 (lower dotted line) to 0.45: 0.27: 0.28 (upper dotted line), the characteristic minimum shifts from 53 ° to 48 °, clearly demonstrating the dependence of the position of the minimum on the composition of the initial atomic orbitals. The theoretical θ dependence due to the matrix element was further multiplied with the XPD of the Mo $3d_{5/2}$ core level to simulate the XPD part of the experimental VB ARXPS result for peak A. The calculated VB ARXPS for peak A [Fig. 4(b)]. On the other hand, the MAOPOP for peak E obtained from the same VB calculation predicted a relatively flat behavior due to more or less evenly populated S $3p$ atomic orbitals with only minor contributions from the Mo $4d$ orbitals. The θ dependence of the matrix element was similarly multiplied by the intensity modulation of the XPD peaks of the Mo $3d_{5/2}$ core level, and an excellent agreement between the experiment and simulated VB ARXPS for peak E was also obtained [Fig. 4(c)].

In the foregoing analysis of the matrix elements, 171 $\mathbf{k}$ points were selected within the triangular net of the surface BZ of $MoS_2(0002)$ to mimic complete BZ averaging during the VB x-ray photoexcitation process. Although the observed independence of the VB XPS peak positions on the polar angle provides experimental evidence that the peak energies and intensities represent averages over the entire BZ, it is important to examine the possible contribution from the incomplete BZ averaging to VB ARXPS. In the direct transition model, the wave vectors parallel to the surface between the initial $\mathbf{k}_{i,\parallel}$ and the final $\mathbf{k}_{f,\parallel}$ states are conserved via $\mathbf{k}_{i,\parallel}=\mathbf{k}_{f,\parallel}-\mathbf{k}_{\mathrm{ph},\parallel}-\mathbf{G}_\parallel$, where $\mathbf{k}_{\mathrm{ph},\parallel}$ is the parallel component of the x-ray photon wave vector and $\mathbf{G}_\parallel$ is a surface reciprocal-lattice vector. Then the experimentally measured final-state wave vector $\mathbf{k}_{f,\parallel}$ at each polar angle can lead directly to the corresponding initial-state wave vector. In the actual ARXPS experiment, a finite acceptance angle of the photoelectron energy analyzer detects the photoelectrons with their wave vectors equal to $\mathbf{k}_{f,\parallel}\pm\Delta\mathbf{k}_{f,\parallel}$, where[3] $|\Delta\mathbf{k}_{f,\parallel}|$ is equal to $[\sqrt{2mE/\hbar^2}\cos\theta\Delta\theta$

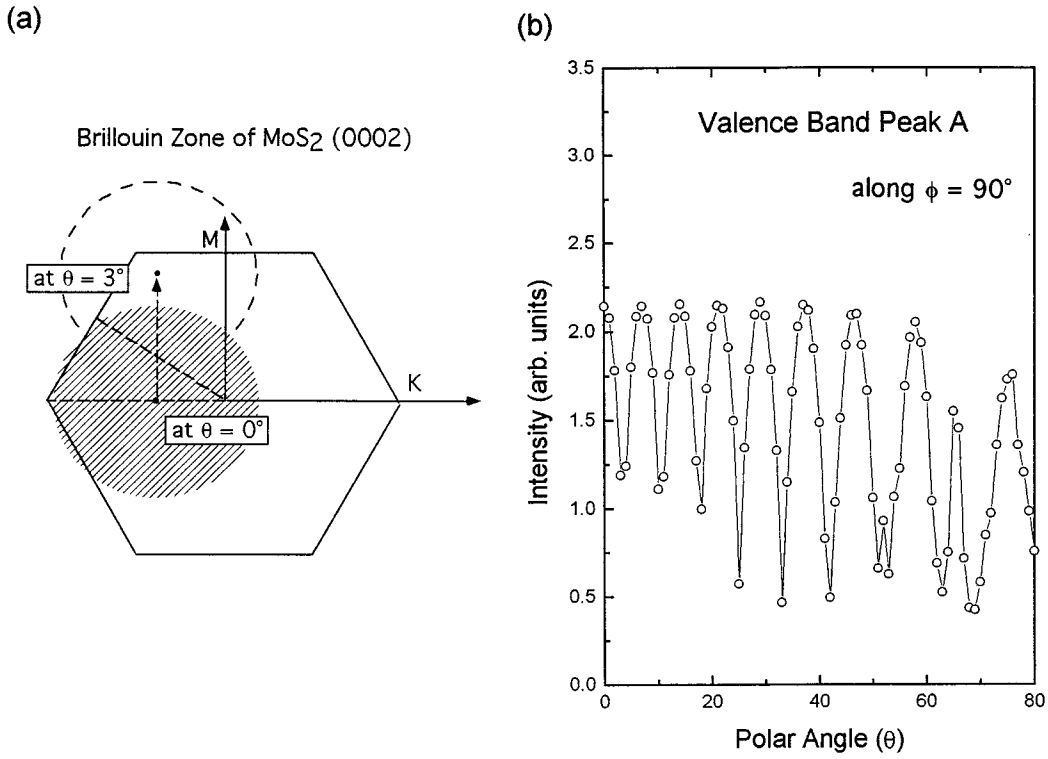

FIG. 6. (a) The ranges of k points for simulating finite-k resolution of the instrument projected on the surface Brillouin zone of MoS_2(0002)—the shaded circle for $\theta=0\,^\circ$ and the dashed circle for $\theta=3\,^\circ$. Note that the centers of the k-point circles are displaced from the line joining the Γ point (or the BZ center) and the M point because of a relatively large value of $|\mathbf{k}_{\rm ph}|$. (b) The calculated direct transition effect on the VB ARXPS for peak A due to the finite-k resolution in our ARXPS.

$+1/2\sqrt{2m/E\hbar^2}\sin\theta\Delta E]$ (in our case, $\Delta\theta=4\,^\circ$ and $\Delta E=0.554$ eV for a pass energy of 300 eV). Therefore, in simulating the partial BZ averaging due to the finite instrument resolution, only the $\mathbf{k}$ points within the radius $|\mathbf{k}_{i,\|}\pm\Delta\mathbf{k}_{i,\|}|$ around $\mathbf{k}_{i,\|}$ at each polar angle θ were included for the calculation of the density of states in the VB. The effect of the incomplete BZ averaging in the calculation of the total density of states (including all five Mo $4d$ and three S $3p$ orbitals) is shown in Fig. 6. At $\theta=0\,^\circ$, all the $\mathbf{k}$ points within the triangular net (bounded within the dashed area) are included, effectively averaging over the whole BZ. On the other hand, at $\theta=3\,^\circ$, a substantial part of the BZ near the Γ point (the BZ center) is not sampled. Consequently, the calculation predicts a large-intensity anisotropy, and further that the intensity decreases rapidly as one moves from the BZ center (e.g., $\theta=0\,^\circ$) to the BZ boundary (e.g., $\theta=3\,^\circ$) [Fig. 6(a)]. The calculated rapid oscillation is the direct consequence of the fact that a small change in the angle θ can cause a sizable change in the initial wave vector due to a large magnitude for the final-state wave vector $|\mathbf{k}_{f,\|}|=\sqrt{2mE/\hbar^2}\sin\theta$ ($\cong 19.7\sin\theta$ Å^{-1} for $E=1480$ eV). Despite the large-intensity anisotropy expected from the incomplete BZ averaging in our ARXPS, the VB ARXPS data show no discernible intensity anisotropy from the direct transition effect. The comparison between the experiment and calculation therefore strongly indicates that the direct transition effect was absent in our VB ARXPS.

The absence of the direct transition effect suggests the importance of the phonon-assisted nondirect transition. In the Debye model of isotropic, thermal vibration, the Debye-Waller attenuation factor can be written as $W(T)\exp(-3\hbar^2g^2T/mk_B\theta_D^2)$, where g is the magnitude of the momentum transfer in the direct transition, and T, m, k_B, and θ_D are the temperature, the mass of the atom, the Boltzmann constant, and the Debye temperature, respectively. The Debye-Waller factor $W(T)$ weighs the direct transition effect relative to the nondirect transition part such that it represents the fraction of transitions which are direct.[12] The Debye temperature of MoS_2 was estimated from specific-heat measurements[24] to be in the range of $\theta_D=260$–320 K. Based on these values of θ_D, a conservative estimate for $W(T)$ ranges from 0.21 to 0.35 with the mass m being equal to the mass of one unit of MoS_2. These values are indeed significantly smaller than 0.55 for tungsten and 0.59 for Ir, in which the direct transition effect was observed to be substantial.[25]

Additional information can be extracted from the VB spectra after recognizing a difference in the XPD's of the Mo $3d_{5/2}$ core and S $3s$ inner VB levels. For the Mo $3d_{5/2}$ core level, the strong forward focusing maximum at $\theta=49\,^\circ$ is the dominant peak, but the S $3s$ level shows a much smaller peak intensity for the same 46 ° direction [Fig. 1(b)]. Therefore, the subsequent intensity ratio $I'_{\rm Mo\ 3d}/I'_{\rm S\ 3s}$ displays a slowly rising trend as the polar angle increases toward $\theta=49\,^\circ$ (top panel in Fig. 7). The difference in the XPD's of the Mo $3d_{5/2}$ core and S $3s$ inner VB levels is not due to the effect of different angular momentum involved in the final states, since a similar result is also obtained when comparing

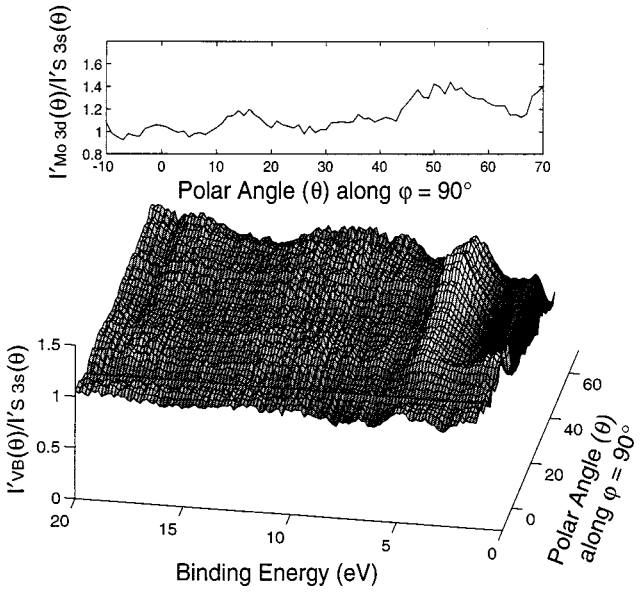

FIG. 7. The VB spectra presented in Fig. 1(a) are divided by the S 3*s* level XPD [Fig. 1(b)]. The result is then compared with the intensity ratio of the Mo $3d_{5/2}$ core level to the S 3*s* level (in the top panel). The deviation of the ratio $I'_{\mathrm{VB}}(\theta)/I'_{\mathrm{S}\,3s}(\theta)$ from the unity results from either intensity anisotropy from the matrix elements or the difference in the XPD patterns from the S and Mo emitters (see the top panel).

the Mo $3d_{5/2}$ and S $2p$ core levels,[15] but is rather due to the geometric inequivalence of the Mo and S emitter positions.[26] The distance to the nearest neighbor along $\theta=0°$ is much larger than that along $\theta=49°$ for the Mo emitter (4.57 Å vs 2.41 Å), while both distances to the nearest scatterers along the two directions are comparable for the S emitter (3.16 Å vs 2.41 Å). Using this difference between the core-level XPD's, the VB and the Mo $3d_{5/2}$ XPD maxima are divided by those of the S 3*s* orbital, and the ratios of $I'_{\mathrm{VB}}/I'_{\mathrm{S}\,3s}$ and $I'_{\mathrm{Mo}\,3d}/I'_{\mathrm{S}\,3s}$ (Ref. 27) are presented in Fig. 7. Intensities vary isotropically, as shown by constant ratio of $I'_{\mathrm{VB}}/I'_{\mathrm{S}\,3s}$ at binding energies corresponding to peaks in the lower portion of the VB, including the region of peak *E*, where the S $3p$ orbitals contribute most (cf. Fig. 5). In the middle portion of the VB (BE≈4.8 eV), the intensity ratio $I'_{\mathrm{VB}}/I'_{\mathrm{S}\,3s}$ shows a small upward deviation from unity for a peak centered at BE=4.8 eV and 49°, similar to the observed ratio $I'_{\mathrm{Mo}\,3d}/I'_{\mathrm{S}\,3s}$ indicating a substantial contribution from a Mo emitter. Near the top of the VB, however, the intensity variation shows a pronounced dip despite the fact that the photoemission from the region mainly originates from the Mo emitters (cf. Fig. 5). This is caused by nonspherically symmetric Mo $4d$ partially filled orbitals. Therefore, unlike in the previous study of the VB XPD from Au/Cu by Stuck *et al.*,[28] we find that the angle dependence of the VB cross sections due to the symmetry of the *d* orbitals cannot be neglected, particularly when the *d* shell is partially filled.

B. Valence-band structure and locus of Cs 6s electrons in Cs/MoS_2

The observed broad maximum at $\theta=0°$ in the VB ARXPS data for the peak designated as the Cs 6*s* level [Fig. 3(a)] is indeed remarkable because such intensity anisotropy from the Cs 6*s* valence level is not expected for the following reasons. First, LEED studies in the literature[29] and our recent investigation of atomic structures at the Cs/MoS_2 interface[15] indicated that Cs adsorption on $MoS_2(0002)$ results in neither a long-range nor a short-range-ordered Cs overlayer. Thus any contribution to the VB ARXPS within the Cs overlayer by a scattering process is unlikely. In fact, the ARXPS of the Cs $4d$ core level also shows no XPD features, supporting the disordered Cs overlayer model [Fig. 3(b)]. In addition, no intensity anisotropy from the electric dipole matrix elements is expected from the Cs 6*s* valence level since the *s* emission only produces an isotropic intensity profile.[7,8] The fact that the experimental intensity anisotropy cannot be adequately described by the expected angularly uniform emission from the Cs 6*s* level forces us to abandon the initial assignment of the Cs-induced valence peak as the Cs 6*s* electrons in a thin overlayer. In fact, our calculation using the SSEHT for Cs/MoS_2 (one Cs atom per each unit cell of MoS_2) indicates a large degree of delocalization of the Cs 6*s* electrons into the MoS_2 substrate, and about 90 % charge transfer from the Cs atom to the substrate. The band-structure calculation (Fig. 8) and the atomic-orbital population analysis predict that the interaction between the Cs 6*s* atomic orbital and the MoS_2 conduction band is substantial near the bottom of the conduction band, whereas the interaction is minimal in the valence-band region including the S 3*s* inner band. At the bottom of the conduction band (~2 eV above peak *A*), the atomic-orbital population mainly consists of empty Mo $4d$ and S $3p$ atomic orbitals with the ratio $4d_{z^2}:4d_{xy}:\ 4d_{x^2-y^2}:\ 3p_x:3p_y:3p_z=0.29:0.24:0.23:0.056:0.066:0.016$ similar to that in clean MoS_2,[14] with a minor contribution from other atomic orbitals including the Cs 6*s* level (0.035) and the total Mo $5p$ level (0.056). From the obtained ratio of the atomic-orbital population, the angle dependence on the matrix element was calculated. Since the Scofield cross sections for the Cs 6*s*, S $3p$, and Mo $5p$ levels are much smaller than that for the Mo $4d$ atomic orbital,[30] the calculated angle dependence on the matrix element largely reflects the relative atomic orbital population

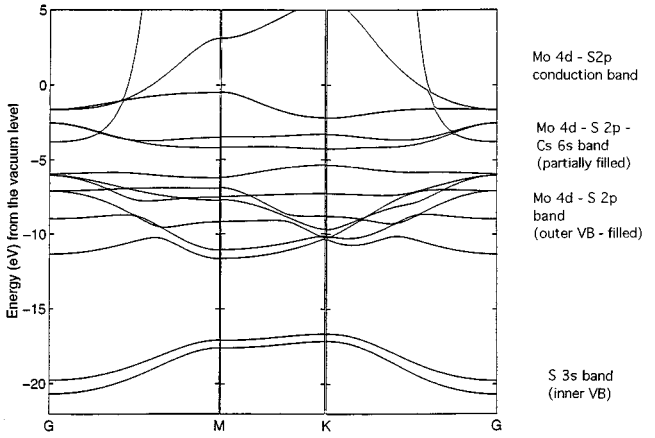

FIG. 8. The VB structure of $Cs/MoS_2(0002)$ calculated with the solid-state extended Hückel theory. One Cs atom was placed above the Mo in each unit cell.

ratio of the Mo $4d$ atomic orbitals. The theoretical intensity anisotropy from the matrix element was subsequently multiplied by the experimental instrument response function[31] to produce the experimentally observed intensity anisotropy for the Cs $6s$ level, and a satisfactory agreement between experiment and theory is observed [solid line, Fig. 3(a)]. In calculating the θ variation of the Cs $4d$ core level, conversely, there is no matrix element contribution from a closed shell. Consequently, the calculated angle dependence of the Cs $4d$ core-level intensities exhibits only a smoothly rising intensity anisotropy, characteristic of electrons localized at a thin Cs overlayer,[32] as observed in experiment [dashed line, Fig. 3(b)].

V. CONCLUSIONS

In this investigation, we found that the VB intensity anisotropy from a clean $MoS_2(0002)$ mainly arises from *both (1) core-electron-like strong forward focusing XPD; and (2) the matrix element contribution due to non-spherically symmetric, partially filled shells.* The contribution from the matrix element can be large enough to alter the total VB intensity anisotropy significantly, and thus must be included to correctly account for the observed angle dependence of the VB intensity. In addition, the observed difference in the core-level XPS's between the Mo and S emitters further provides experimental means to decompose the VB to contributions from the Mo and S atoms at specific energies in the valence band. The Cs adsorption on the basal plane of clean MoS_2 (with a Cs coverage of 0.23 ML) introduces a Cs-induced peak at 1.25 eV above the VB maximum. A comparison between the experimental intensity anisotropy of the Cs-induced valence level and the theory indicates that the observed angle dependence of the valence level results from the intensity variation due to the electric dipole matrix element at the bottom of the conduction band in the MoS_2 substrate, *suggesting delocalization of the Cs 6s electrons into the Mo S_2 substrate.*

ACKNOWLEDGMENTS

We are grateful to A. Miller of the SCIENTA ESCA laboratory for the time allocation and technical assistance, and the financial support from the Department of Energy Basic Energy Sciences under grant No. DE-FG02-86ER13580.

*Present address: Department of Chemistry, West Virginia University, Morgantown, WV 26506.

[1] K. Siegbahn, U. Gelius, H. Siegbahn, and E. Olson, Phys. Scr. **1**, 272 (1970).

[2] W. L. Schaich, in *Photoemission in Solids I*, edited by M. Cardona and L. Ley (Springer-Verlag, Berlin, 1978), p. 105.

[3] N. V. Smith, in *Photoemission in Solids I* (Ref. 2), p. 242.

[4] F. R. McFeely, J. Stohr, G. Apai, P. S. Wehner, and D. A. Shirley, Phys. Rev. B **14**, 3273 (1976).

[5] R. H. Williams, P. C. Kemeny, and L. Ley, Solid State Commun. **19**, 495 (1976).

[6] J. W. Gadzuk, Solid State Commun. **15**, 1011 (1974); J. W. Gadzuk, Phys. Rev. B **10**, 5030 (1974).

[7] J. W. Gadzuk, Phys. Rev. B **12**, 5608 (1975).

[8] S. M. Goldberg, C. S. Fadley, and S. Kono, J. Electron. Spectrosc. Relat. Phenom. **21**, 285 (1981).

[9] R. J. Baird, L. F. Wagner, and C. S. Fadley, Phys. Rev. Lett. **37**, 111 (1976).

[10] Z. Hussain, E. Umbach, J. J. Barton, J. G. Tobin, and D. A. Shirley, Phys. Rev. B **25**, 672 (1982).

[11] J. Osterwalder, T. Greber, S. Hufner, and L. Schlapbach, Phys. Rev. Lett. **64**, 2683 (1990).

[12] G. S. Herman, T. T. Tran, K. Higashiyama, and C. S. Fadley, Phys. Rev. Lett. **68**, 1204 (1992).

[13] R. Mamy, A. Boufelja, and B. Carricaburu, Phys. Status Solidi B **141**, 467 (1987), and references therein.

[14] M. Richards-Babb, Ph. D. thesis, Lehigh University, 1993, and references therein.

[15] K. T. Park, M. Richards-Babb, M. Freund, J. Weiss, and K. Klier, J. Phys. Chem. **100**, 10 139 (1996).

[16] *Scienta ESCA300 User's Manual* (Scienta, Uppsala, Sweden, 1989).

[17] For a general review of forward focusing phenomena, see W. F. Egelhoff, Jr., CRC Crit. Rev. Solid State Mater. Sci. **16**, 213 (1990).

[18] Linear background was removed for the Mo $3d_{5/2}$ and S $3s$ levels and Shirley background for the VB peaks. The intensities of the VB peaks A–E presented in Fig. 1(b) are the integrated areas of the VB peaks fitted with a Voight function—a linear combination of Gaussian and Lorentzian peak shapes. A method to extract the VB intensities by considering the peak maxima only was also examined, and both methods yielded a consistent result.

[19] C. Y. Su, I. Lindau, P. W. Chye, S.-J. Oh, and W. E. Spicer, J. Electron Spectrosc. Relat. Phenom. **31**, 221 (1983).

[20] *Handbook of X-ray Photoelectron Spectroscopy,* edited by J. Chastain (Perkin-Elmer, Eden Prairie, Minnesota, 1992).

[21] The atomic-orbital population for the valence band was calculated with the solid-state extended Hückel theory and then multiplied by the Scofield cross section to simulate VB XPS spectra. See also Ref. 14 and J. H. Scofield, J. Electron. Spectrosc. Relat. Phenom. **8**, 129 (1981).

[22] The relative atomic-orbital population was normalized to the total atomic orbital population. Note that Ref. 14 uses unnormalized atomic-orbital population.

[23] J. Hess, K. Park, and K. Klier (unpublished).

[24] *Specific Heat-Nonmetallic Solids,* in Thermophysical Properties of Matter: The TPRC Data Series, Vol. 5, edited by Y. S. Touloukian and E. H. Buyco (IFI/Plenum, New York, 1970), p. 690.

[25] Z. Hussain, C. S. Fadley, S. Kono, and L. F. Wagner, Phys. Rev. B **22**, 3750 (1982).

[26] We note the difference of ~5% between the kinetic energies of the Mo $3d_{5/2}$ (1257 eV) and S $2p$ (1324 eV) core levels, although such a small difference is unlikely to cause the observed difference in the XPD of the two core levels.

[27] The intensities $I_{VB}(\theta)$ and $I_{S\,3s}(\theta)$ are first divided by their values at $\theta=0°$ to yield $I'_{VB}(\theta)=I_{VB}(\theta)/I_{VB}(0°)$ and $I'_{S\,3s}(\theta)=I_{S\,3s}(\theta)/I_{S\,3s}(0°)$. Then the intensity ratio $I'_{VB}(\theta)/I'_{S\,3s}(\theta)$ is obtained.

[28] A. Stuck, J. Osterwalder, T. Greber, S. Hüfner, and L. Schlap-

bach, Phys. Rev. Lett. **65**, 3029 (1990).
[29] C. A. Papageogopoulos, Surf. Sci. **75**, 17 (1978).
[30] The Scofield cross sections for the Mo $4d$, S $3p$, and Cs $6s$ levels are 0.2033, 0.0774, and 0.0059, respectively, in units of 13 600 barns (1 barn$=1\times10^{-28}$ m^2).
[31] The instrument response function was extracted from a smooth nonforward focusing background intensity profile in the Mo $3d_{5/2}$ core-level XPD.
[32] W. A. Fraser, J. V. Florio, W. N. Delgass, and W. D. Robertson, Surf. Sci. **36**, 661 (1973).